



Trans. Nonferrous Met. Soc. China 31(2021) 3416-3427

Transactions of Nonferrous Metals Society of China

www.tnmsc.cn



Dynamic recrystallization and silicide precipitation behavior of titanium matrix composites under different strains

Er-tuan ZHAO¹, Shi-chen SUN¹, Jin-rui YU¹, Yu-kun AN¹, Wen-zhen CHEN², Rui-run CHEN³

- 1. School of Mechanical Engineering, Shandong University of Technology, Zibo 255022, China;
- 2. School of Materials Science and Engineering, Harbin Institute of Technology, Weihai 264209, China;
 - 3. National Key Laboratory for Precision Hot Processing of Metals, Harbin Institute of Technology, Harbin 150001, China

Received 14 September 2021; accepted 10 November 2021

Abstract: In order to elucidate the microstructure evolution and silicide precipitation behavior during high-temperature deformation, TiB reinforced titanium matrix composites were subjected to isothermal hot compression at 950 °C, strain rate of 0.05 s^{-1} and employing different strains of 0.04, 0.40, 0.70 and 1.00. The results show that with the increase of strain, a decrease in the content, dynamic recrystallization of the α phase and the vertical distribution of TiB along the compression axis lead to stress stability. Meantime, continuous dynamic recrystallization reduces the orientation difference of the primary α phase, which weakens the texture strength of the matrix. The recrystallization mechanisms are strain-induced grain boundary migration and particle stimulated nucleation by TiB. The silicide of Ti₆Si₃ is mainly distributed at the interface of TiB and α phase. The precipitation of silicide is affected by element diffusion, and TiB whisker accelerates the precipitation behavior of silicide by hindering the movement of dislocations and providing nucleation particles.

Key words: titanium matrix composites; dynamic recrystallization; silicide precipitation; hot compression

1 Introduction

Titanium matrix composites are typical aerospace materials that are used due to their excellent mechanical properties, especially high-temperature strength [1–4]. In-situ TiB reinforced titanium matrix composites have attracted wide attention since they overcome the drawback of poor wettability between reinforcement and matrix [5,6]. However, the introduction of TiB whiskers and the formation of coarse Widmanstatten structure during solidification decreases the plasticity of titanium matrix composites. The hot working method can improve plasticity and increase strength [7,8]. It is noticeable that the results of hot working are related to the original microstructure, strain, deformation

temperature, and deformation rate [8-10]. PENG et al [11] established the relationship among flow stress, strain rate, and deformation temperature of Ti60 titanium alloy. They noticed that to avoid instability such as cracking, the strain rate should not be higher than 1 s⁻¹ during hot working. So, it is clear that the strain has an important effect on the evolution of microstructure and deformation behavior of titanium matrix composites. Still, the reported investigations are mainly directed on the microstructure when the flow stress reaches a steady state to understand deformation rate and temperature's effect on formability [12]. Despite this, only a little attention is paid to the effect of strain on microstructural evolution. Hence, based on earlier studies on the effects of temperature and strain rate on the deformation behavior [13], they

are selected as 950 °C and 0.05 s⁻¹, respectively. Also, the effects of recrystallization and silicide precipitation on the deformation behavior are studied. In addition to the formability, many investigations also emphasize improving mechanical properties of the titanium matrix composites [14]. The mechanical properties at room temperature of titanium matrix composites with poorly plastic hexagonal close-packed structure α phase depend on the formation of texture during hot working [15-17]. Then, the texture strength increases sharply with the deepening strain. The study on the evolution of texture during hot working is significant in controlling the α phase and morphological orientation of TiB to improve the mechanical properties. Thus, studies on the textural evolution of TiB reinforced titanium matrix composites, and the precipitation behavior of silicides are necessary.

The hot working process often accompanies silicide precipitation, and it usually occurs in the $\alpha+\beta$ phase region [18]. The abundant Zr and Si elements in the β phase provide favorable conditions for the silicide precipitation. The precipitated silicide can hinder the movement of dislocations and promote the recrystallization behavior of the matrix. ZHANG et al [19] found that silicide increases the deformation activation energy of Ti65 high-temperature titanium alloy, making the deformation difficult. This indicates that the silicide precipitation further worsens the processability of titanium matrix composites. The precipitation of silicide during multi-directional forging has been reported [20], but the effect of TiB on silicide precipitation during hot compression has not been explored. This necessitates studying effect of TiB on precipitation behavior of silicide in the deformation process of TiB reinforced titanium matrix composites.

In this study, the microstructural evolution and silicide precipitation behavior at the TiB interface of titanium matrix composites are elucidated using the hot compression test at different strains. The recrystallization behavior of α phase under flow stress is studied, and the effect of TiB on silicide precipitation behavior is discussed. The mechanism of recrystallization and silicide precipitation during hot compression is clarified. From the results obtained from the present work, valuable insights about the deformation mechanism and silicide

precipitation behavior of the titanium matrix composites are received.

2 Experimental

A nominal composition of Ti-6Al-4Sn-10Zr-1Mo-1Nb-1W-0.3Si (wt.%) and 3 vol.% TiB reinforced phase titanium matrix composites with β transition temperature of 1000 °C were prepared by vacuum induction melting. Briefly, a sample of size $d8 \text{ mm} \times 12 \text{ mm}$ was cut from the ingot, and graphite slices were placed at both ends for lubrication. The hot compression test for the ingot was conducted using the Gleeble-1500 simulator. As per the reported data [13], the conditions for hot compression were set as temperature of 950 °C, strain rate of 0.05 s⁻¹, and the varied applied strains as 0.04, 0.40, 0.70, and 1.00. The sample was preheated for 5 min before the hot compression test and subjected to water quenching immediately after the completion of the test. To eliminate the effect of heating temperature on the evolution of microstructure and silicide precipitation, a control group was designed with heat treatment experiments for hot compression experiments. The as-cast samples were quenched directly without applying pressure after heat treatment for 400 and 420 s. An area was selected and prepared for the microstructural observation as per the procedure reported in Ref. [13]. The amorphous colloidal silica polishing suspension (MasterMet2) was used to polish the surface using a vibration polishing machine (Buehler VibroMet 2). The microstructure of titanium matrix composites observed using backscattering scanning electron microscopy (BSEM, FEI Quanta 250), electron backscatter diffraction (EBSD), and transmission electron microscopy (TEM, Tecnai G2 F20S). Based on the results of EBSD, the density of dislocations (ρ) can be roughly estimated using Eq. (1) [21]:

$$\rho = \kappa/b$$
 (1)

where κ is the lattice curvature, *b* is the Burgers vector, and the value is 2.95×10^{-10} for α phase.

3 Results and discussion

3.1 Stress-strain curve during hot compression

As shown in Fig. 1, the microstructure analysis

confirms the presence of TiB whisker, residual β phase, and primary α phase. Defects such as casting shrinkage cavities are observed in the matrix which are shown by the arrows.

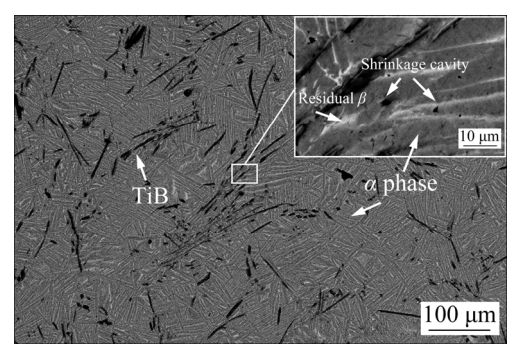


Fig. 1 As-cast microstructure of titanium matrix composite

The stress-strain curves of titanium matrix composites under different strains (0.04, 0.40, 0.70 and 1.00) shown in Fig. 2 assist in understanding the trend in stress change during the hot compression test. The four stress-strain curves under different strains depict a similar trend, indicating that the observation of microstructural evolution by the semi-in-situ route is reliable. Before the strain reaches 0.04 (Fig. 2(a)), the stress increases gradually to 128.93 MPa along with the strain due to the work hardening effect. Once the stress reaches the maximum, the dynamic softening rate becomes higher than the machine hardening rate, and thus, stress is reduced (Figs. 2(b-d)). When the strain reaches about 0.70 (Fig. 2(c)), the stress-strain curve attains dynamic equilibrium. Above this point, the stress does not change significantly with the increase in strain (Fig. 2(d)).

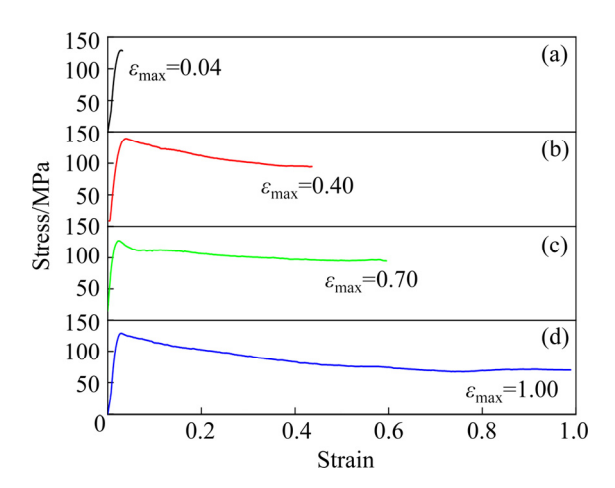


Fig. 2 Stress-strain curves at various strains: (a) 0.04; (b) 0.40; (c) 0.70; (d) 1.00

3.2 Microstructural evolution

The microstructures of the control group after heat treatment are shown in Fig. 3. After heat treatment for 400 s, the content of the primary α phase decreases, and silicide is mainly distributed at the interface between the primary α phase and residual β phase. During the rapid cooling process after the heat treatment, the silicide adheres to the interface of the primary α phase instead of competing with the β phase [22]. With the increase of the heat treatment time, the morphology and content of the primary α phase vary slightly, and the morphology of some silicides at the termination position evolves from granular to thin shells. The high chemical potential energy and element diffusion rate at the termination position may be responsible for the formation of thin shell silicide.

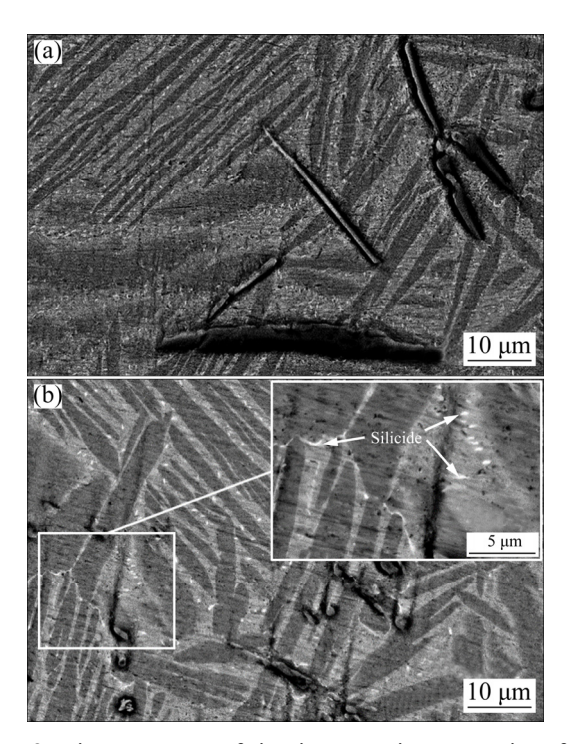


Fig. 3 Microstructure of titanium matrix composite after heat treatment for 400 s (a) and 420 s (b)

The microstructures of titanium matrix composite under different strains are presented in Fig. 4. It is found that the content of the primary α phase decreases, and also, silicide precipitates mainly settle at the boundary of the primary α phase. Due to the good plasticity of the matrix at 950 °C, the crushing degree of TiB whiskers increases slightly with the increase in applied strain. Also, it is noted that the increased residual β phase developed during hot compression is retained after

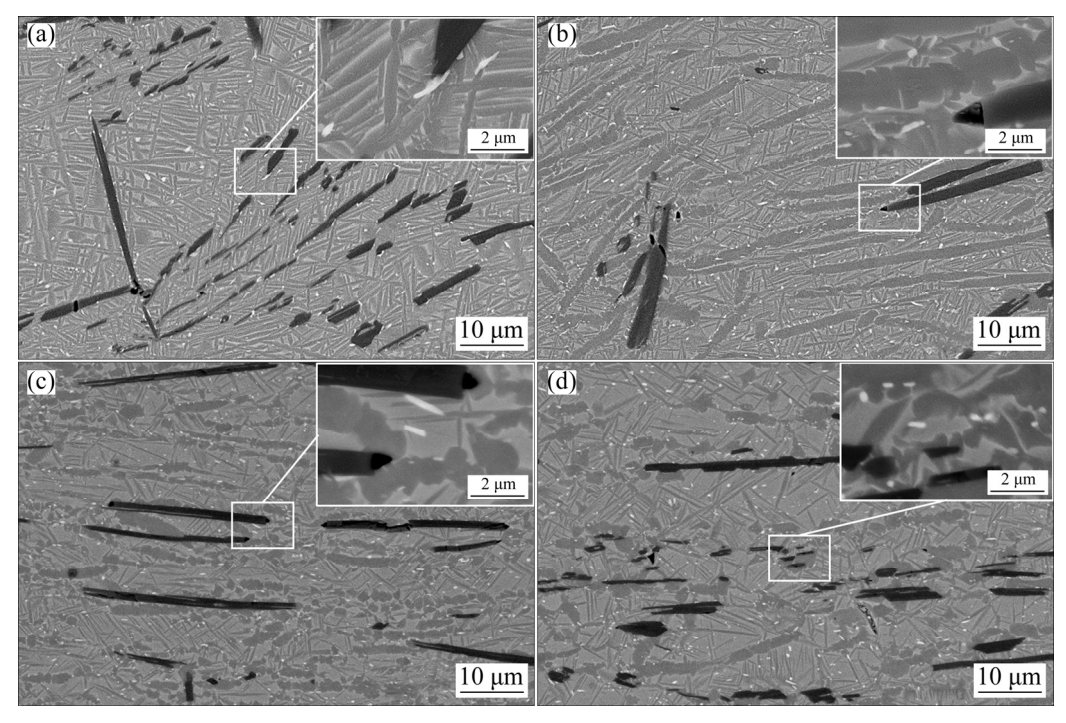


Fig. 4 Microstructures of titanium matrix composite subjected to various strains: (a) 0.04; (b) 0.40; (c) 0.70; (d) 1.00

the water quenching process. As the content of the β phase becomes higher, the processability of titanium matrix composites is improved [23] and provides favorable conditions for silicide precipitation [24,25]. The stress approaches the peak value when the strain is 0.04 (Fig. 4(a)), and the recrystallization degree is relatively low. The lamellar primary α phase is retained in the matrix. Most TiB whiskers are intact, and some voids are present due to a few broken TiB junctions. Further, the β phase is transformed into the α phase in the subsequent cooling process. When the strain is 0.40, the primary α phase recrystallizes. Still, due to the limited deformation when the strain is 0.40, only a small quantity of the equiaxed α phase is observed in Fig. 4(b). The interface of the primary α phase is curved in the magnified image (Fig. 4(b)), and the serrated α phase boundary produced by the grain boundary migration provides a nucleation position [26], which can accelerate the recrystallization process [27]. The mechanism of this recrystallization is referred to as strain-induced grain boundary migration [28].

Although the degree of deflection and fragmentation of TiB whiskers are increased compared to Fig. 4(a), it is not completely perpendicular to the compression axis. From Fig. 4(c), some lamellar primary α phases can be

observed when the stress is stable (ε =0.70), and there is an apparent increase in the number of equiaxed α phases. The broken TiB whisker is perpendicular to the compression axis. With further increase of strain to 1.00, the primary α phase is further equiaxed; only a very small amount of lamellar primary α phase is observed in the matrix. In the magnified image (Fig. 4(d)), a part of the equiaxed α phase at the interface of TiB whiskers displays that the second phase can promote recrystallization. This mechanism is termed as particle stimulated nucleation [29,30]. It should be noted that the stress can be related to the orientation of TiB whiskers in the matrix when the stress reaches stability (Fig. 2), the orientation of TiB whiskers no longer changes (Fig. 4). Compared to the microstructure after heat treatment (control group), the thin shell silicide at the α phase boundary disappears during deformation. With the progress of deformation, the gradual decrease in the content of the primary α phase indicates that the temperature of the material increases [31]. It is reported that the increase in temperature leads to the spheroidization of thin shell silicide [22]. Therefore, the lack of timely loss of heat generated during deformation may be the main reason for the disappearance of thin shell silicide.

To further observe the evolution of the

microstructure and sub-structure during the titanium matrix composites deformation, characterized using EBSD. Under thermal stress, the β grains are refined, and the size of α clusters is decreased. The inverse pole figure (IPF, Fig. 5(a)) displays that the orientation of the secondary α phase in the same α cluster is consistent, and a disorder exists between different α clusters and compression axis. No dense peaks could be observed in the corresponding pole figure (PF) (Fig. 5(b)). When the strain increases to 0.4, the primary α phase begins to recrystallize (Fig. 5(c)). The peak intensity of the Position A decreases (Fig. 5(b)). Some high-intensity peaks appear along the direction of RD (Fig. 5(d)), indicating the preferred orientation in the matrix. Figures 5(e) and (g) demonstrate IPFs at strains 0.70 and 1.00, respectively. With the progress of compression, α cluster size further decreases and is identified as a grain at the position illustrated in the ellipsoid. The preferred orientation is not further expanded or even slightly reduced (Figs. 5(f) and (h)), which might be related to the recrystallization of the lamellar primary α phase.

The cumulative misorientations along the long axis of the lamellar α phase are shown in Fig. 6.

The cumulative misorientations are counted along the arrow direction in all the illustrations, and the left endpoint is the starting point. It can be seen from Fig. 6(a) that when the strain is 0.04, the cumulative misorientations of the lamellar α phase are less than 2°, while all adjacent misorientations are also less than 2°. CHEN et al [32] proposed that the orientation deviation of less than 2° could be attributed to the formation of low angle grain boundaries (LAGBs) caused by the accumulation of dislocations. Hence, it can be concluded that the lamellar α phase is relatively stable when the strain is low, and therefore, the softer β phase's dislocations are difficult to spread in the α phase to produce effective deformation [33]. When the strain increases to 0.40, the cumulative orientation deviation along the L2 line gradually increases in the lamellar α phase, as shown in Fig. 6(b). Several small directional jumps (no more than 5°) are recorded which imply the proliferation of many dislocations. A continuous increase in the cumulative misorientations shows that the sub-grain boundaries continuously capture the dislocations with increased strain. The sub-grain boundary inside the lamellar α phase gradually becomes active. It can be deduced from Fig. 6(c) that when

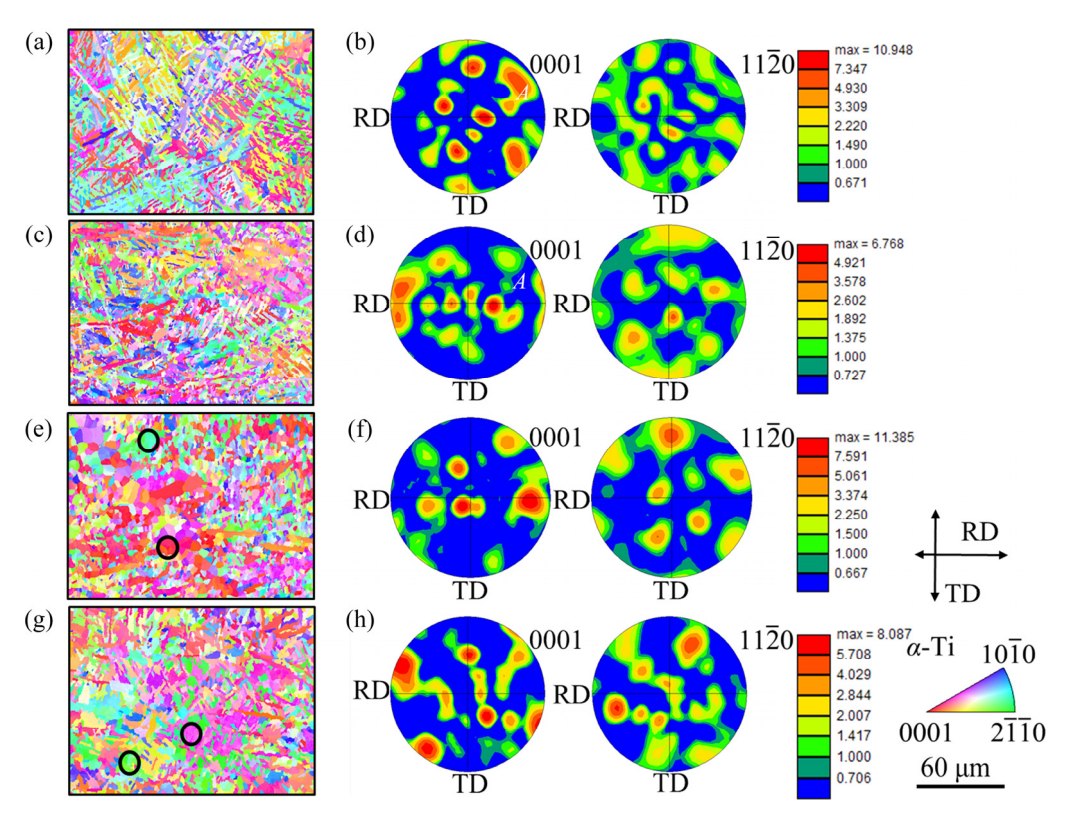


Fig. 5 EBSD maps together with pole figures of α phase at different strains: (a, b) 0.04; (c, d) 0.40; (e, f) 0.70; (g, h) 1.00; (a, c, e, g) IPF; (b, d, f, h) PF

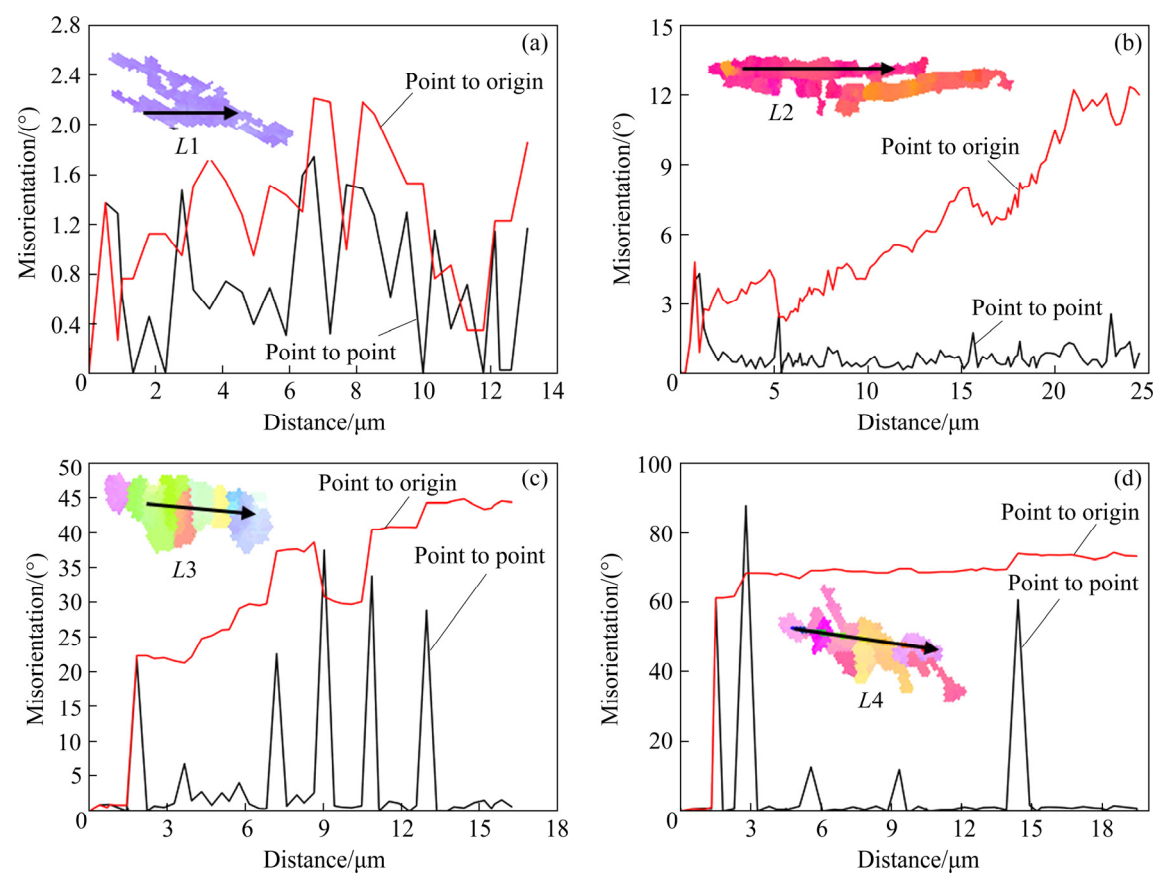


Fig. 6 Evolution of misorientation gradient along straight lines in lamellar α phase at different strains: (a) 0.04; (b) 0.40; (c) 0.70; (d) 1.00

the strain is 0.70, the orientation difference between the adjacent grains is large, and the point-to-point orientation difference reaches 35°, which is significantly more than 15°. However, the orientation difference is relatively stable within the sub-grain. This is consistent with the results of HUANG and LOG [34] that the formation of new sub-grains is due to the transformation from LAGBs to high angle grain boundaries (HAGBs). At a strain of 1.00, very few lamellar α phases exist in the matrix. From the grain analysis shown in Fig. 6(d), it is clear that the lamellar α phase is divided into multiple segments. According to the cumulative orientation difference, it can be substantiated that the new recrystallized α phase is formed in the lamellar α phase. It is noticeable from the variation trend of cumulative misorientations that the strain promotes the formation of HAGBs, which is an important feature of the recrystallization process. This process of forming complete recrystallized grains is called as continuous dynamic recrystallization (CDRX) [35]. In the hot compression test, the CDRX is mainly

responsible for the refinement of the α phase in the titanium matrix composites.

It can be inferred from Fig. 6 that the recrystallization of the lamellar α phase occurs during hot compression, characterized by gradual rotation of sub-grain orientation. Figure 7 displays the variation in the dislocation density of titanium matrix composites calculated under different strains using Eq. (1). The dislocation density increases with an increase in strain, and the rate of increase is higher in the strain range of 0.40–0.70. Combined with the stress–strain curve (Fig. 2), the dynamic recrystallization rate is most significant in this range. As a result, with the accumulation of dislocations during hot compression, the sub-grain orientation in the lamellar α phase changes and gradually evolves into recrystallized grains.

As shown in Fig. 8(a), except for the interfacial bending of a few lamellar α phases, the micromorphology of α clusters is not deformed, indicating that the recrystallization in titanium matrix composites is very limited at a strain of 0.04. It is worth noting that when the strain increases to

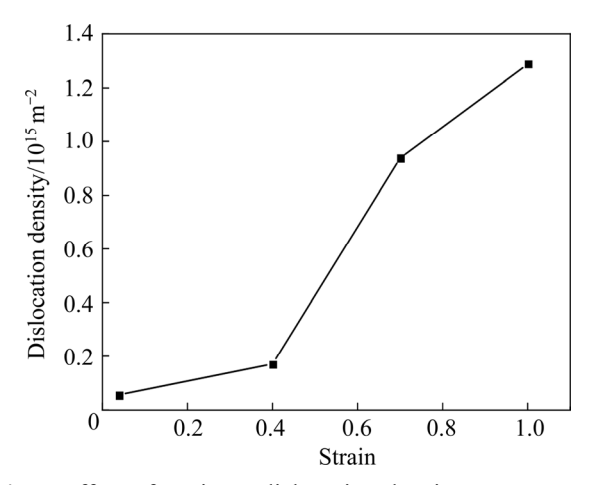


Fig. 7 Effect of strain on dislocation density

0.40, the lamellar α phase is cut into two parts by silicide (from the selected area electron diffraction (SAED) results) or other oriented α phases (Fig. 8(b)). Also, it is inferred that the second phase like silicide easily becomes the nucleation particles for recrystallized grains, which accelerates the recrystallization process. With progress deformation, the coarse lamellar α phase is refined into fine equiaxed grains, as indicated in the dotted line in Fig. 8(c). In the deformation process, dislocations gather at the α phase boundary, leading to new sub-grains and eventually evolving into new recrystallized grains. With a continuous increase in the strain to 1.00 (Fig. 8(d)), the recrystallized grains completely replace the lamellar α phase.

3.3 Precipitation behavior of silicide

The solubility of silicon near the primary α phase can be expressed by the Thompson-Freundlich equation (Eq. (2)) as follows [36]:

$$\ln(C_{\rm r}/C_{\infty}) = 2M_{\rm p}\gamma/(RT\rho r) \tag{2}$$

where $C_{\rm r}$ represents the equilibrium solubility of silicon, C_{∞} represents the solubility at the end of the primary α phase, M_p is the molar mass, γ is the interface energy, R is the gas constant, T is the thermodynamic temperature, ρ is the density, and ris the radius of curvature at the termination. With the increase in heat treatment time, the primary α phase in the as-cast structure gradually declines. The increase of r leads to the increase of the potential energy of silicon at the end of the α phase, which accelerates the diffusion of solute atoms, leading to the formation of high chemical potential at the end of the α phase. Therefore, thin shell silicide is easier to form at the terminal ends during heat treatment. Figure 9 shows the elemental distribution obtained by line scanning of EDS at the α/β phase boundary and the terminal end of the primary α phase. As shown by the dotted line in Fig. 9(c), the peaks of Si, Nb, and Mo elements near silicide appear simultaneously. This phenomenon is more apparent near the thin shell silicide at the terminal end of the primary α phase. During the heat treatment, α phase transforms into β phase, and Nb and Mo as β stable elements diffuse to α

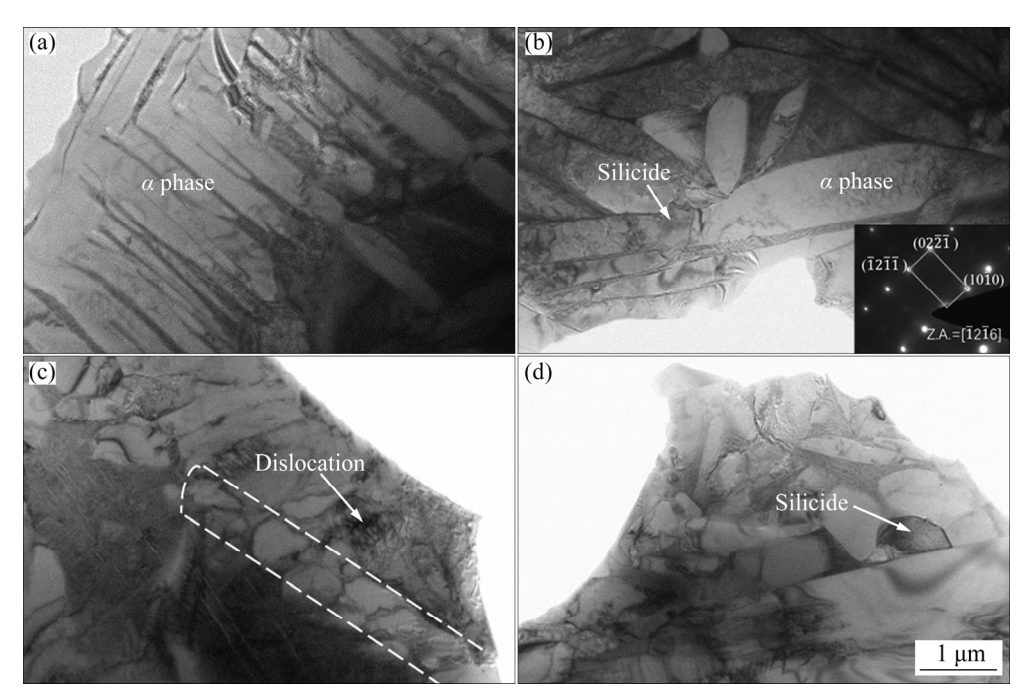


Fig. 8 TEM micrographs of lamellar α phase at different strains: (a) 0.04; (b) 0.40; (c) 0.70; (d) 1.00

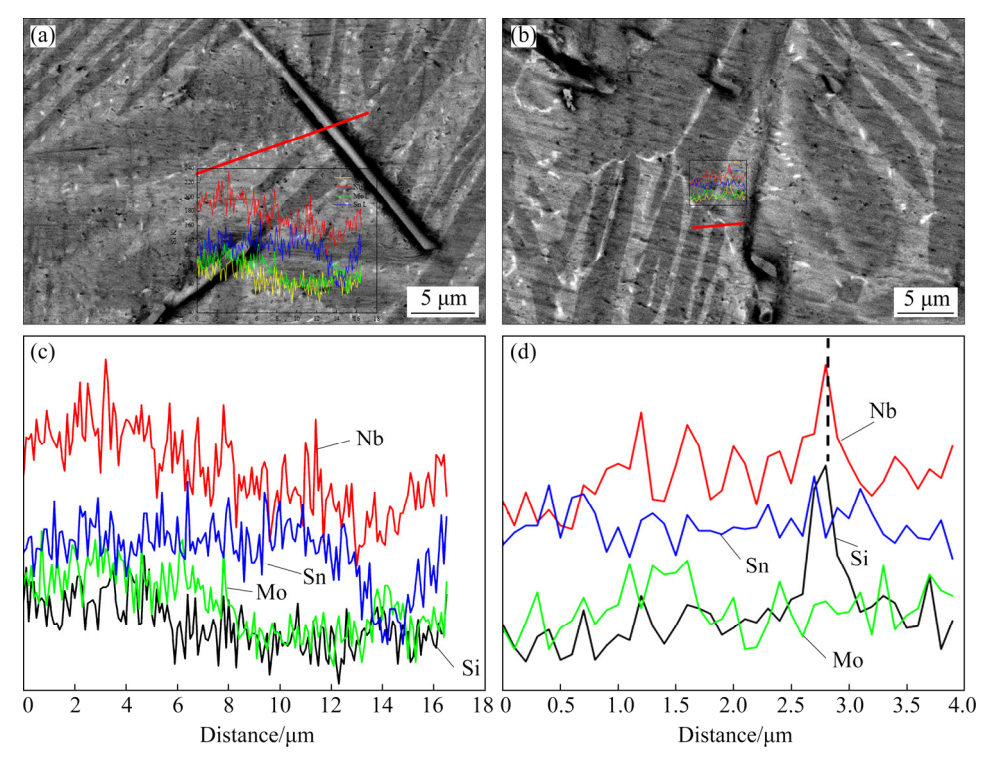


Fig. 9 Line scan positions of titanium matrix composites after heat treatment at 400 s (a) and 420 s (b), and line scan results at 400 s (c) and 420 s (d)

interface, providing favorable conditions for silicide precipitation. On the other hand, the phase transition occurs easily near the terminal end of the α phase, and therefore, thin shell silicide first forms near the terminal end.

Besides precipitating at the interface of the primary α phase, silicide could also be observed at the interface of the TiB whiskers, especially at the termination of the whisker during hot compression. Taking titanium matrix composites subjected to a strain of 0.7 (Fig. 2(c)) as an example, the precipitation behavior of nano-silicide near TiB is observed using TEM. As displayed in Fig. 10(a), silicide shows an average size of 400 nm at the interface of TiB whiskers. Corresponding to this position, it is evident from HRTEM (Fig. 10(b)) that there is a ledge with a height of about 10 nm in the direction of the {010} plane of TiB, indicating that the in-situ TiB whiskers grow by the ledge mechanism. The ledge at the TiB interface can provide more nucleation particles, making it easier for silicide to nucleate and grow along the ledge. Moreover, due to the stress introduced by hot compression, stress stripes (Fig. 10(b)) produced at the interface between TiB whisker and silicide, which is consistent with the direction of the {010} crystal face of TiB. The magnified image (Fig. 10(c)) clearly shows that the lattice distortion produced by TiB whiskers during hot compression and the introduction of dislocation on the ledges can be retained by water quenching. composition supercooling of interstitial Si atom, which easily spreads and aggregates along dislocations is another important reason for silicide precipitation at the interface of TiB whiskers. Thus, the ledge at the interface of TiB whiskers and the stress during compression accelerate the precipitation behavior of silicide. Lattice distortion of TiB is caused by stress, and the dislocation is introduced to the ledge at the phase boundary of TiB. The silicon element diffuses and accumulates rapidly along the dislocations at the phase boundary and causes supercooling.

The protruding phase boundary ledges facilitate the precipitation of silicide, making it easier to nucleate and grow. The crystal face spacings D1 and D2 of TiB whiskers measured from Fig. 10(c) are 0.200 and 0.217 nm, respectively, and the crystal face spacings of silicide are 0.219 and 0.237 nm, respectively. Based on this, the mismatches between the silicide and $\{010\}$ crystal face and the $\{\overline{1}00\}$ crystal face of the TiB whisker are estimated to be 9.5% and 9.2%, respectively. The large degree of mismatch

indicates that the crystal plane between them is non-coherent. Figure 10(d) is the fast Fourier transform (FFT) image of Fig. 10(c). The satellite spots around the reflection of the TiB whisker crystal face from the interference between the silicide $\{1\,\overline{1}01\}$ and $\{01\,\overline{12}\}$ crystal faces and the TiB $\{010\}$ and $\{\overline{1}00\}$ crystal faces also imply that the interface between them is incoherent. Combined

with the EDS energy spectrum (Fig. 10(e)) and existing reports [37], it is further confirmed that the type of silicide precipitated is Ti₆Si₃.

According to the microstructure evolution of titanium matrix composites during hot compression, the schematic for the recrystallization process is depicted, as shown in Fig. 11. In the initial state (Fig. 11(a)), the matrix structure consists of the

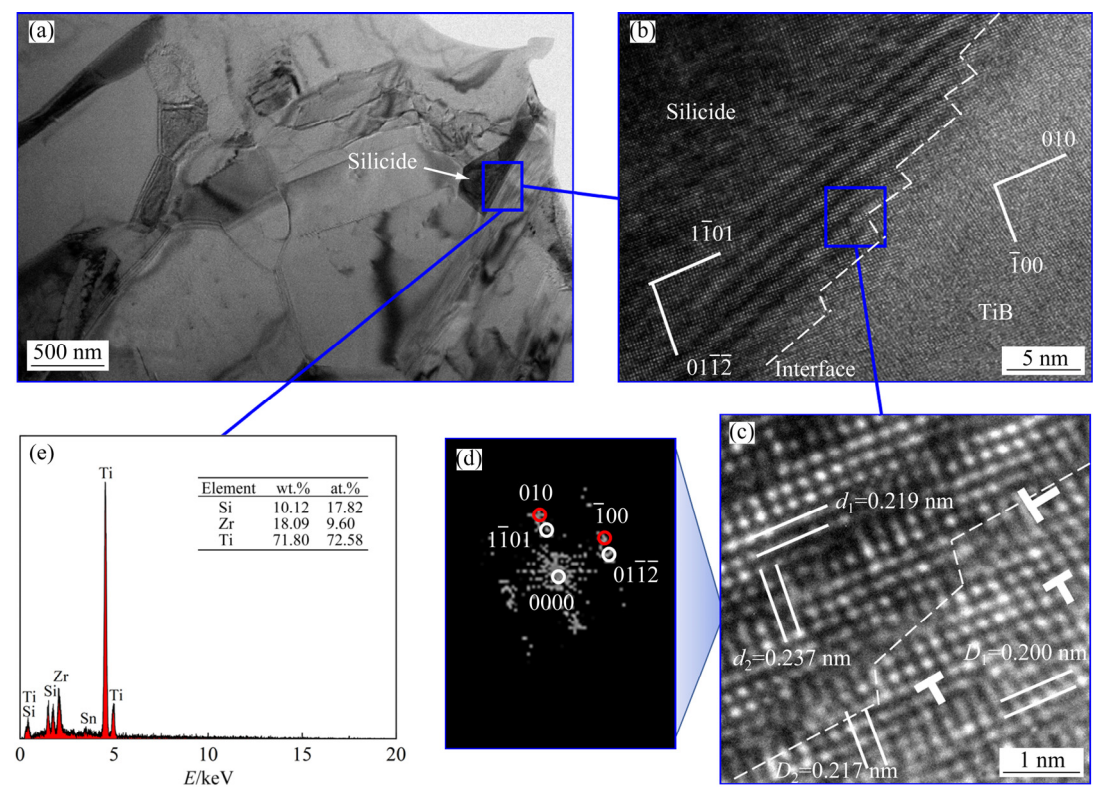


Fig. 10 TEM image (a) and HRTEM images of interface (b, c), fast Fourier transform image (d), and EDS energy spectrum of silicide (e)

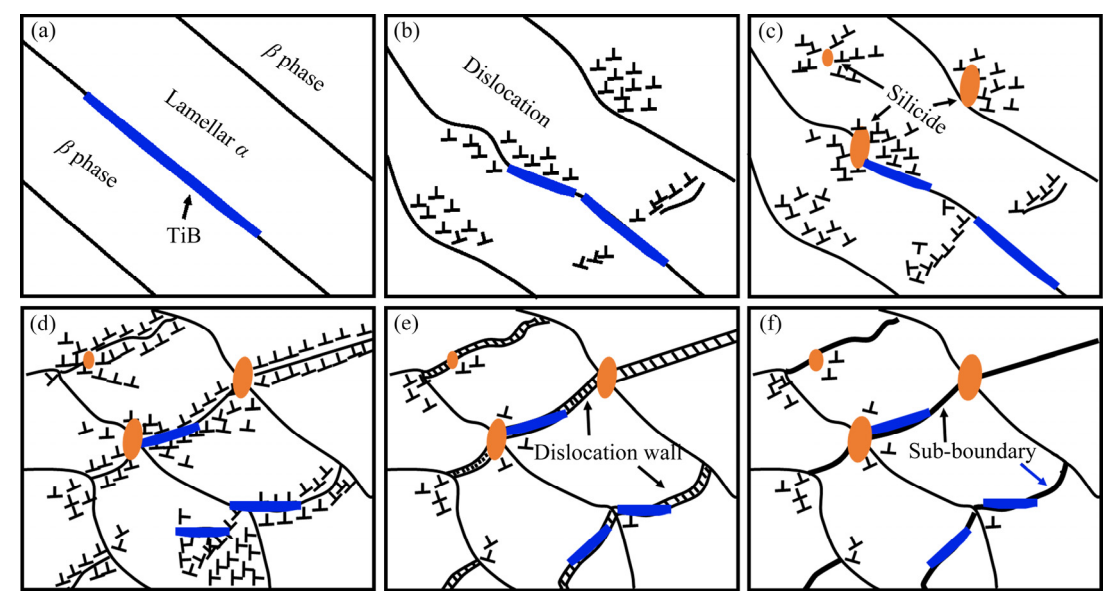


Fig. 11 Schematic diagram of recrystallization: (a) Original microstructure; (b) Dislocation generation; (c) Dislocation multiplication; (d) Dislocation accumulation; (e) Dislocation wall; (f) Subgrain formation

primary α phase, β phase, and the silicide produced in the heat preservation. At the beginning of hot compression (Fig. 11(b)), a part of the TiB strengthening phase is broken under the applied load, the lamellar α phase deflects, and the dislocations accumulate at the α phase boundary, silicide, and TiB. With the increase in strain (Figs. 11(c, d)), dislocations accumulate in the lamellar α phase to form sub-grains, misorientation gradient between the adjacent sub-grains increases, and silicide precipitates at the α phase boundary and TIB. As the strain increases continuously (Fig. 11(e)), the dislocation wall forms in the original primary α phase, the silicide size becomes larger, and the TiB distributes along the direction perpendicular to the compression axis. Finally, the accumulated dislocations form a phase boundary, as shown in Fig. 11(f). The dynamic recrystallization reduces the dislocation density and transforms the lamellar α phase into an equiaxed α phase.

4 Conclusions

- (1) With an increase in strain, the silicide content precipitated at the boundary between TiB whisker and α phase changes slightly, while the recrystallization degree of the primary α phase increases. The mechanism of continuous dynamic recrystallization can be classified as strain-induced grain boundary migration of the α phase and particle-stimulated nucleation by TiB whisker.
- (2) The recrystallization of the α phase results in a decrease in texture strength and preferred orientation. Recrystallization during the hot compression is mainly responsible for grain refinement. The cumulative misorientations display that the formation of recrystallized grains results from the transformation of LAGBs to HAGBs.
- (3) Element diffusion is the main reason for silicide precipitation, and the interface between TiB and Ti₆Si₃ silicide is incoherent. The dislocation deposited near the TiB whiskers accelerates silicon diffusion, and the ledge at the interface provides nucleation particles, offering favorable conditions for silicide precipitation.

Acknowledgments

The authors are grateful for the financial supports from the National Natural Science

Foundation of China (No. 51871184), the Natural Science Foundation of Shandong Province, China (No. ZR2019MEM037), the Zhoucun School-City Integration Development Plan, China (No. 2020ZCXCZH03), and the School-city Integration Development Project of Zibo, China (No. 2019ZBXC022).

References

- [1] HUANG L L, PENG H, KAVEENDRAN B. High temperature tensile properties of in situ TiB_w/Ti6Al4V composites with a novel network reinforcement architecture [J]. Materials Science and Engineering A, 2012, 534: 688-692.
- [2] CAI Chao, HE Shan, LI Li-fan, TENG Qing, SONG Bo, YAN Chun-ze, WEI Qing-song, SHI Yu-sheng. In-situ TiB/Ti-6Al-4V composites with a tailored architecture produced by hot isostatic pressing: Microstructure evolution, enhanced tensile properties and strengthening mechanisms [J]. Composites (Part B): Engineering, 2019, 164: 546-558.
- [3] ZHANG Jin-yong, KE Wen-xuan, JI Wei, FAN Zhang, WANG Wei-ming, FU Zheng-yi. Microstructure and properties of insitu titanium boride (TiB)/titanium (TI) composites [J]. Materials Science and Engineering A, 2015, 648: 158–163.
- [4] HUANG Li-qing, WANG Li-hua, QIAN Ma, ZOU Jin. High tensile-strength and ductile titanium matrix composites strengthened by TiB nanowires [J]. Scripta Materialia. 2017, 141: 133–137.
- [5] LIN Ying-hua, JIANG Chang-chun, LIN Zhen-heng, CHEN Qing-tang, LEI Yong-ping, FU Han-guang. Laser in-situ synthesis of high aspect ratio TiB fiber bundle reinforced titanium matrix composite coating [J]. Optics & Laser Technology, 2019, 115: 364–373.
- [6] GAISIN R, IMAYEV V, IMAYEV R. Effect of hot forging on microstructure and mechanical properties of near α titanium alloy/TiB composites produced by casting [J]. Journal of Alloys and Compounds, 2017, 723: 385–394.
- [7] WANG X, ZHAN M, GAO P, MA P, YANG K, LEI Y, LI Z. Deformation mode dependent mechanism and kinetics of dynamic recrystallization in hot working of titanium alloy [J]. Materials Science and Engineering A, 2020, 772: 138804.
- [8] ZHAO Q, YANG F, TORRENS R, BOLZONI L. Evaluation of the hot workability and deformation mechanisms for a metastable beta titanium alloy prepared from powder [J]. Materials Characterization, 2019, 149: 226–238.
- [9] BALASUNDAR I, RAGHU T, KASHYAP B. Hot working and geometric dynamic recrystallisation behaviour of a near-α titanium alloy with acicular microstructure [J]. Materials Science and Engineering A, 2014, 600: 135–144.
- [10] ZHAO Z, WANG Q, LIU J, YANG R. Effect of heat treatment on the crystallographic orientation evolution in a near-α titanium alloy Ti60 [J]. Acta Materialia, 2017, 131: 305–314.
- [11] PENG Wen-wen, ZENG Wei-dong, WANG Qing-jiang, YU Han-qing. Characterization of high-temperature deformation

- behavior of as-cast Ti60 titanium alloy using processing map [J]. Materials Science and Engineering A, 2013, 571: 116–122.
- [12] MUTOMBO K, SIYASIYA C, STUMPF W. Diffusional transformation in Ti6Al4V alloy during isothermal compression [J]. Transactions of Nonferrous Metals Society of China, 2019, 29(10): 2078–2089.
- [13] SUN Shi-chen, ZHAO Er-tuan, HU Chen, TIAN Yu-jing, CHEN Wen-zhen, CUI Hong-zhi, CHEN Rui-run. Deformation behavior and softening mechanism of TiB reinforced near-alpha titanium matrix composite during hot compression [J]. Journal of Materials Research and Technology, 2020, 9(6): 13250-13263.
- [14] MORAKABATI M, HAJARI A. Hot working behavior of near alpha titanium alloy analyzed by mechanical testing and processing map [J]. Transactions of Nonferrous Metals Society of China, 2020, 30(6): 1560-1573.
- [15] DU Zhao-xin, HE Qi-wei, CHEN Rui-run, LIU Fei, ZHANG Jing-yong, YANG Fei, ZHAO Xue-ping, CUI Xiao-ming, CHENG Jun. Rolling reduction-dependent deformation mechanisms and tensile properties in a β titanium alloy [J]. Journal of Materials Science & Technology, 2022, 104: 183–193
- [16] WU Yong, FAN Rong-lei, QIN Zhong-huan, CHEN Ming-he. Shape controlling and property optimization of TA32 titanium alloy thin-walled part prepared by hot forming [J]. Transactions of Nonferrous Metals Society of China, 2021, 31(8): 2336–2357.
- [17] FAN Rong-lei, WU Yong, CHEN Ming-he, XIE Lan-sheng. Relationship among microstructure, mechanical properties and texture of TA32 titanium alloy sheets during hot tensile deformation [J]. Transactions of Nonferrous Metals Society of China, 2020, 30(4): 928–943.
- [18] ZHAO Er-tuan, SUN Shi-chen, ZHANG Yu. Recent advances in silicon containing high temperature titanium alloys [J]. Journal of Materials Research and Technology, 2021, 14: 3029–3042.
- [19] ZHANG Zhi-xin, FAN Jiang-kun, TANG Bin, KOU Hong-chao, WANG Jian, WANG Xin, WANG Shi-ying, WANG Qing-jiang, CHEN Zhi-yong, LI Jin-shan. Microstructural evolution and FCC twinning behavior during hot deformation of high temperature titanium alloy Ti65 [J]. Journal of Materials Science & Technology, 2020, 49: 56-69.
- [20] SUN Shi-chen, ZHAO Er-tuan, HU Chen, AN Yu-kun, CHEN Wen-zhen. Precipitation behavior of silicide and synergetic strengthening mechanisms in TiB-reinforced high-temperature titanium matrix composites during multi-directional forging [J]. Journal of Alloys and Compounds, 2021, 867: 159051.
- [21] DILLIEN S, SEEFELDT M, ALLAIN S, BOUAZIZ O, HOUTTE P. EBSD study of the substructure development with cold deformation of dual phase steel [J]. Materials Science and Engineering A, 2010, 527(4/5): 947–953.
- [22] LUO X, LIU L H, YANG C, LU H Z, MA H W, WANG Z, LI D D, ZHANG L C, LI Y Y. Overcoming the strengthductility trade-off by tailoring grain-boundary metastable Si-containing phase in β-type titanium alloy [J]. Journal of Materials Science & Technology, 2021, 68: 112–123.

- [23] VO P, JAHAZI M, YUE S, BOCHER P. Flow stress prediction during hot working of near- α titanium alloys [J]. Materials Science and Engineering A. 2007, 447(1/2): 99–110.
- [24] DAVIES P, PEDERSON R, COLEMAN M, BIROSCA S. The hierarchy of microstructure parameters affecting the tensile ductility in centrifugally cast and forged Ti-834 alloy during high temperature exposure in air [J]. Acta Materialia, 2016, 117: 51-67.
- [25] SU Y, HAO G J, FAN H Y, ZHAI Y W, KONG F T, WANG X P, CHEN Y Y. Study on rolling of a new near-α titanium alloy: Microstructure refinement and dual-scale silicides evolution [J]. Journal of Alloys and Compounds, 2020, 852: 156867.
- [26] LIU Zhang-guang, LI Pei-jie, XIONG Liang-tong, LIU Tai-ying, HE Liang-ju. High-temperature tensile deformation behavior and microstructure evolution of Ti55 titanium alloy [J]. Materials Science and Engineering A, 2017, 680: 259–269.
- [27] WANG Ke, WU Ming-yu, REN Zhao, ZHANG Yu, XIN Ren-long, LIU Qing. Static globularization and grain morphology evolution of α and β phases during annealing of hot-rolled TC21 titanium alloy [J]. Transactions of Nonferrous Metals Society of China, 2021, 31(9): 2664–2676.
- [28] LI J S, DONG R F, KOU H C, FAN J K, ZHU B, TANG B. Texture evolution and the recrystallization behavior in a near β titanium alloy Ti-7333 during the hot-rolling process [J]. Materials Characterization, 2019, 159: 109999.
- [29] IMANDOUST A, BARRETT C, OPPEDAL A, WHITTINGTON W, KADIRI H. Nucleation and preferential growth mechanism of recrystallization texture in high purity binary magnesium—rare earth alloys [J]. Acta Materialia, 2017, 138: 27–41.
- [30] BALL E, PRANGNELL P. Tensile-compressive yield asymmetries in high strength wrought magnesium alloys [J]. Scripta Metallurgica Et Materialia, 1994, 31(2): 111–116.
- [31] HONG S, LMYA B, YCLA B, LYZA B, CXLA B, HJLA B, JFW C. Effect of heat treatment processing on microstructure and tensile properties of Ti-6Al-4V-10Nb alloy [J]. Transactions of Nonferrous Metals Society of China, 2019, 29(1): 59-66.
- [32] CHEN R, TAN C W, YU X D, HUI S X, LEE Y T. Effect of TiB particles on the beta recrystallization behavior of the Ti-2Al-9.2Mo-2Fe-0.1B metastable beta titanium alloy [J]. Materials Characterization, 2019, 153: 24-33.
- [33] WANG Ke, WU Ming-yu, YAN Zhi-bing, LI Dong-rong, XIN Ren-long, LIU Qing. Dynamic restoration and deformation heterogeneity during hot deformation of a duplex-structure TC21 titanium alloy [J]. Materials Science and Engineering A, 2018, 712: 440–452.
- [34] HUANG K, LOG R. A review of dynamic recrystallization phenomena in metallic materials [J]. Materials & Design, 2016, 111: 548–574.
- [35] LI L, LUO J C, YAN J J, LI M Q. Dynamic globularization and restoration mechanism of Ti-5Al-2Sn-2Zr-4Mo-4Cr alloy during isothermal compression [J]. Journal of Alloys and Compounds, 2015, 622: 174-183.

- [36] DONG Z, LU K, HU Z. Formation and stability of a supersaturated solid solution phase formed during a melt-spinning process [J]. Nanostructured Materials, 1999, 11(3): 351–360.
- [37] FU Bin-guo, WANG Hong-wei, ZOU Chun-ming, WEI Zun-jie. The influence of Zr content on microstructure and precipitation of silicide in as-cast near *α* titanium alloys [J]. Materials Characterization, 2015, 99: 17–24.

不同应变下钛基复合材料的动态再结晶和硅化物析出行为

赵而团1, 孙世臣1, 于金瑞1, 安钰坤1, 陈文振2, 陈瑞润3

- 1. 山东理工大学 机械工程学院,淄博 255022;
- 2. 哈尔滨工业大学 材料科学与工程学院, 威海 264209;
- 3. 哈尔滨工业大学 金属精密热加工国家重点实验室,哈尔滨 150001

摘 要:为了研究 TiB 增强钛基复合材料在高温变形过程中的组织演变和硅化物析出行为,950 °C 时在应变速率为 $0.05~{\rm s}^{-1}$,应变分别为 0.04、0.40、0.70 和 1.00 的工况下对其进行等温热压缩试验。研究发现:随着应变的增加,初生 α 相含量降低及其发生的连续动态再结晶和 TiB 增强相沿垂直压缩轴方向的定向分布导致应力趋于稳定,同时连续动态再结晶导致初生 α 相的取向差减小,从而削弱基体的织构强度。动态再结晶的机制主要是应变诱导晶界迁移以及 TiB 增强相诱导晶粒形核。元素扩散促进硅化物的析出,析出的 Ti₆Si₃型硅化物主要分布在 TiB 及 α 相的界面上,TiB 增强相通过阻碍位错的运动和提供形核质点加速硅化物的析出行为。

关键词: 钛基复合材料; 动态再结晶; 硅化物析出; 热压缩

(Edited by Xiang-qun LI)